Synthesis of Ce−Fe Intermetallic Compounds with Foam Structures via Electrochemical Deposition

Gao-Ren Li,*,†,‡ Qin-Fang Ke,† Zi-Shou Zhang,† Ci-Ren Dawa,† Peng Liu,† Guan-Kun Liu,† and Ye-Xiang Tong*,†

MOE of Key Laboratory of Bioinorganic and Synthetic Chemistry, School of Chemistry and Chemical Engineering, Institute of Optoelectronic and Functional Composite Materials, Sun Yat-Sen University, Guangzhou 510275, P. R. China, and State Key Lab of Rare Earth Materials Chemistry and Applications, Beijing 100871, P. R. China

Received September 15, 2006. Revised Manuscript Received January 13, 2007

Cyclic voltammetry was used to investigate the electrochemical behaviors of Fe(II) and Ce(III) in 3.00 mol/L urea−dimethylsulfoxide (DMSO). The electrode processes of Fe(II) and Ce(III) reducing on Pt electrodes were irreversible steps. Experimental results showed that Fe(II) in 3.00 mol/L urea−DMSO could induce the electrodeposition of Ce(III). The Ce−Fe intermetallic compounds with foam structures were successfully obtained by potentiostatic electrodeposition in the 0.01 mol/L $Ce(CH_3SO_3)_3$−0.01 mol/L $FeCl_2$−3.00 mol/L urea−DMSO system. The concentrations of the salts and hydrogen ions have much effect on the pore number and wall structure of the foam. The effect of the potential of electrodeposition, Fe^{2+} concentration, and the ratio of the concentrations of Ce^{3+} to Fe^{2+} in the deposition solution on the contents of Ce in Ce−Fe intermetallic compounds were investigated in our paper. The electrodeposited Ce−Fe intermetallic compounds were amorphous as proved by X-ray diffraction analysis (XRD).

1. Introduction

Cerium intermetallic compounds exhibit a wide variety of interesting ground states, ranging from magnetically ordered and superconducting with unconventional pairing to valence fluctuating and "Kondo insulator" behavior.[1−6] It is well-known that controlling the morphological properties of materials during synthesis is of great importance, as these structural characteristics strongly influence the performance and purpose of the materials.

In the past decade, there has been the tendency toward the development of novel, well-structured, porous, and high-surface-area nanostructures with different shapes and sizes because of their corresponding novel properties and potential applications. For instance, dye-sensitized photovoltaic cells, dimensionally stable anodes (DSA), metal-ion batteries, electrochemical supercapacitors, hydrogen storage devices, and bio- and gas sensors require the development of new functional porous materials to achieve better and optimized performances.[7−13] Increasing the number of pores on the surface is an effective way to greatly increase the specific surface area. At present, a number of methods have been developed for fabricating high-surface-area porous materials, among which the electrochemical method provides a simple and efficient path.[14−16] The growth rates and compositions of deposits can easily be controlled by deposition potentials, current densities, and salt concentrations. Recently, Shin et al. have reported a novel way of producing unique self-supported 3D foams of metals (such as copper and tin) with highly porous ramified walls in aqueous electrolytes by electrochemical deposition accompanying hydrogen evolution, which has been deliberately suppressed in typical electrodeposition processes to produce dense metallic components.[14,15] However, at present, the fabrication of rare earth−transition metal intermetallic compounds with highly porous structures is still a great challenge for material scientists. The oxidation−reduction potentials of rare earth elements are very negative, and it is very difficult to electrodeposit rare earth intermetallic compounds from aqueous electrolytes. Therefore, nonaqueous solvents are usually used. Organic solvents are of great interest for electrochemical purposes because they have wide electro-

* Corresponding author. E-mail: ligaoren@mail.sysu.edu.cn; chedhx@mail.sysu.edu.cn.
† Sun Yat-Sen University.
‡ State Key Lab of Rare Earth Materials Chemistry and Applications.

(1) Macaluso, R. T.; Moreno, N. O.; Fisk, Z.; Thompson, J. D.; Chan, J. Y. *Chem. Mater.* **2004**, *16*, 1560−1563.
(2) Gaudin, E.; Chevalier, B.; Heying, B.; Rodewald, U. C.; Pottgen, R. *Chem. Mater.* **2005**, *17*, 2693−2700.
(3) Kraft, R.; Pottgen, R.; Kaczorowski, D. *Chem. Mater.* **2003**, *15*, 2998−3002.
(4) Chevalier, B.; Bobet, J.-L.; Pasturel, M.; Bauer, E.; Weill, F.; Decourt, R.; Etourneau, J. *Chem. Mater.* **2003**, *15*, 2181−2185.
(5) Tsvyashchenko, A. V.; Ryasny, G. K.; Komissarova, B. A.; Fomicheva, L. N.; Sorokin, A. A. *Solid State Commun.* **2005**, *135*, 373−376.
(6) Gil, A.; Penc, B.; Gondek, L.; Szytula, A.; Hernandez-Velasco, J. *J. Alloys Compd.* **2002**, *346*, 43−46.
(7) Tosheva, L.; Valtchev, V. P. *Chem. Mater.* **2005**, *17*, 2494.
(8) Stein, A. *Adv. Mater.* **2003**, *15*, 763.
(9) Taguchi, A.; Schüth, F. *Microporous Mesoporous Mater.* **2005**, *77*, 1.
(10) Schüth, F. *Chem. Mater.* **2001**, *13*, 3184.
(11) Scott, B. J.; Wirnsberger, G.; Stucky, G. D. *Chem. Mater.* **2001**, *13*, 3140.
(12) Sanchez, C.; Lebeau, B.; Chaput, F.; Boilot, J. P. *Adv. Mater.* **2003**, *15*, 1969.
(13) Vayssieres, L.; Keis, K.; Hagfeldt, A.; Lindquist, S.-E. *Chem. Mater.* **2001**, *13*, 4698.
(14) Shin, H. C.; Liu, M. *Chem. Mater.* **2004**, *16*, 5460−5464.
(15) Shin, H. C.; Liu, M. *Adv. Funct. Mater.* **2005**, *15*, 582−586.
(16) Shin, H. C.; Jiang, D.; Liu, M. *Adv. Mater.* **2003**, *15*, 1610.

10.1021/cm062206q CCC: $37.00
Published on Web 04/04/2007

chemical windows that can reach values of more than 5 V, depending on substrate. Thus, they allow access to many elements and compounds, especially to active metal materials that otherwise cannot be electrodeposited from aqueous solutions, such as rare earth metals. The DMSO system shows a high chemical and thermal stability as well as wide electrochemical windows and is a good medium for the electrodeposition of rare earth intermetallic compounds. Herein, we report a simple method for the synthesis of porous Ce−Fe intermetallic compounds with foam structures in an organic bath with hydrogen bubbles functioning as a dynamic template.

2. Experimental Section

The dehydrated $Ce(CH_3SO_3)_3$ was obtained by the reaction of Ce_2O_3 (99.99%) with CH_3SO_3H (AR) and H_2O_2 and dehydration in a vacuum at 353.15 K. Before use, DMSO (AR) was dehydrated with 4 Å molecular sieves and distilled under a reduced pressure to remove impurities.

The electrochemical experiments were carried out in a simple three-electrode glass cell. The working electrodes were platinum (99.99%) or copper (99.99%) and had an area of 0.08 cm^2. A platinum foil was used as a counter-electrode. A saturated calomel electrode (SCE) was used as the reference electrode that was connected to the cell with a double salt bridge system. All potential values determined in this study were the values versus SCE. The electrochemical deposition experiments were carried out in an organic bath containing 0.01 mol/L $FeCl_2$−3.00 mol/L urea−DMSO, 0.01 mol/L $Ce(CH_3SO_3)_3$−3.00 mol/L urea−DMSO, and 0.01 mol/L $Ce(CH_3SO_3)_3$−0.01 mol/L $FeCl_2$−3.00 mol/L urea−DMSO. Argon was flushed through the bath, and the argon flow was maintained over the solution during the measurements.

The voltammetry experiments were done with a Zahner Elektrik IM6e electrochemical workstation. All the experiments were carried out at a temperature of 298 K. The prepared Ce−Fe intermetallic compounds were analyzed by X-ray energy dispersive spectroscopy (EDS) to determine the contents of cerium and iron, and X-ray diffraction (XRD) to determine the structures. The surface morphologies were observed with scanning electron microscopy (SEM).

3. Results and Discussion

Figure 1a shows the cyclic voltammograms of Pt electrodes in 0.01 mol/L $FeCl_2$−3.00 mol/L urea−DMSO at 298 K at different sweep rates. There was a cathodic wave appearing in every cyclic voltammogram, and the cathodic wave corresponded to the reduction of Fe(II), namely, Fe(II) + $2e^- \rightarrow$ Fe. On the reverse sweep, there was also an anodic peak appearing in every cyclic voltammogram that corresponded to the oxidation of Fe. The peak potential of the cathodic wave (E_p) shifted negatively with increasing sweep rates (v), as shown in Figure 1a. The plot of E_p versus the natural logarithm of v exhibited a linear variation (Figure 1b), and the peak current of cathodic wave (i_p) increased linearly with increasing $v^{1/2}$ (Figure 1c). All these characteristics indicated that the reduction of Fe(II) was irreversible. For an irreversible charge-transfer electrode process, the plot of E_p−ln v was a straight line with a slope $k = RT/2anF$, and $|E_{P/2} - E_P| = 1.857RT/(\alpha nF)$ can be obtained.[17] ($E_{P/2}$ and α stand for the half peak potential and electron-transfer coefficient, respectively). So the transfer coefficient a = 0.076 was calculated from the slope of the plot of E_p versus ln v shown in Figure 1b. From Figure 1a, we could obtain $E_{P/2}$ and E_P, and α = 0.082 can be obtained. According to the relationship of i_p with v at 298 K, $i_p = 2.99 \times 10^5 n^{3/2}\alpha^{1/2}AcD^{1/2}v^{1/2}$ was obtained[17] (i_p, A, and D stand for peak current, electrode area, and diffusion coefficient, respectively). $D = 4.24 \times 10^{-10}$ m^2 s^{-1} can be calculated from the plot of i_p versus $v^{1/2}$ for the reduction peak shown in Figure 1c.

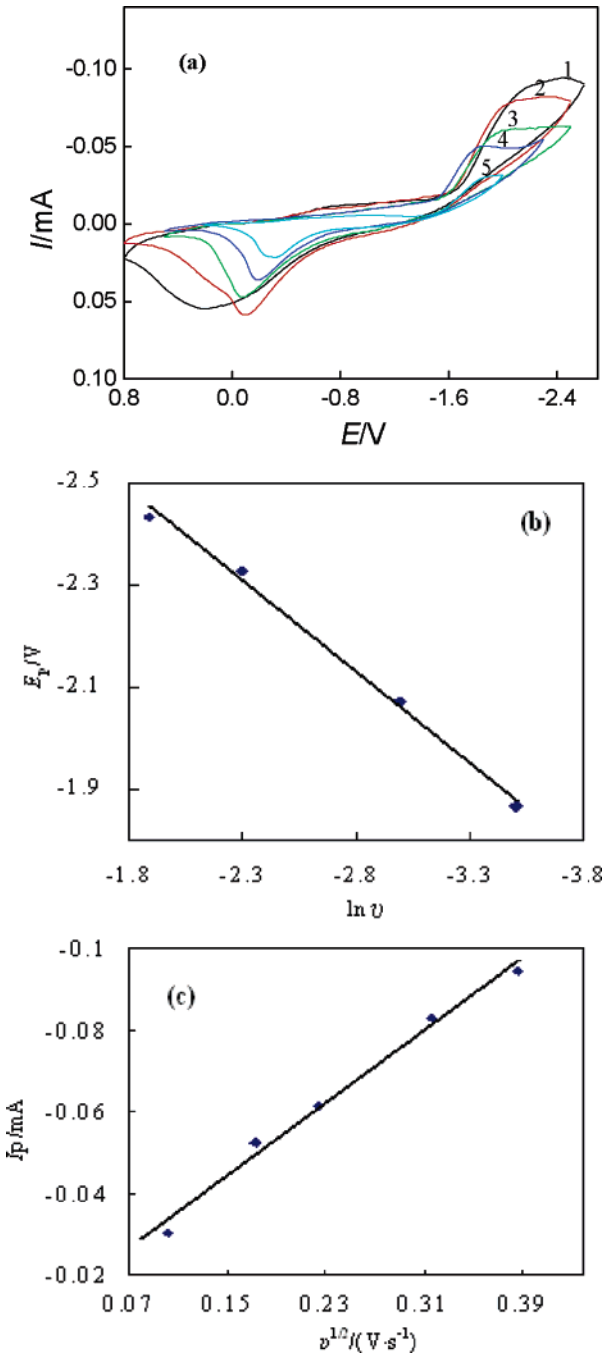

Figure 1. (a) Cyclic voltammograms of Pt electrodes in 0.01 mol/L $FeCl_2$−3.00 mol/L urea−DMSO (0.08 cm^2) at different sweep rates (T = 298 K, v/(mV s^{-1}): (1) 150, (2) 100, (3) 50, (4) 50, (5) 30); (b) E_{pc}−ln v curve; (c) I_p−$v^{1/2}$ curve.

(17) Bard, A. J.; Faulkner, L. R. *Electrochemical Methods*; John Wiley & Sons: New York, 1980; pp 33, 195, 222, 223, 253, 298.

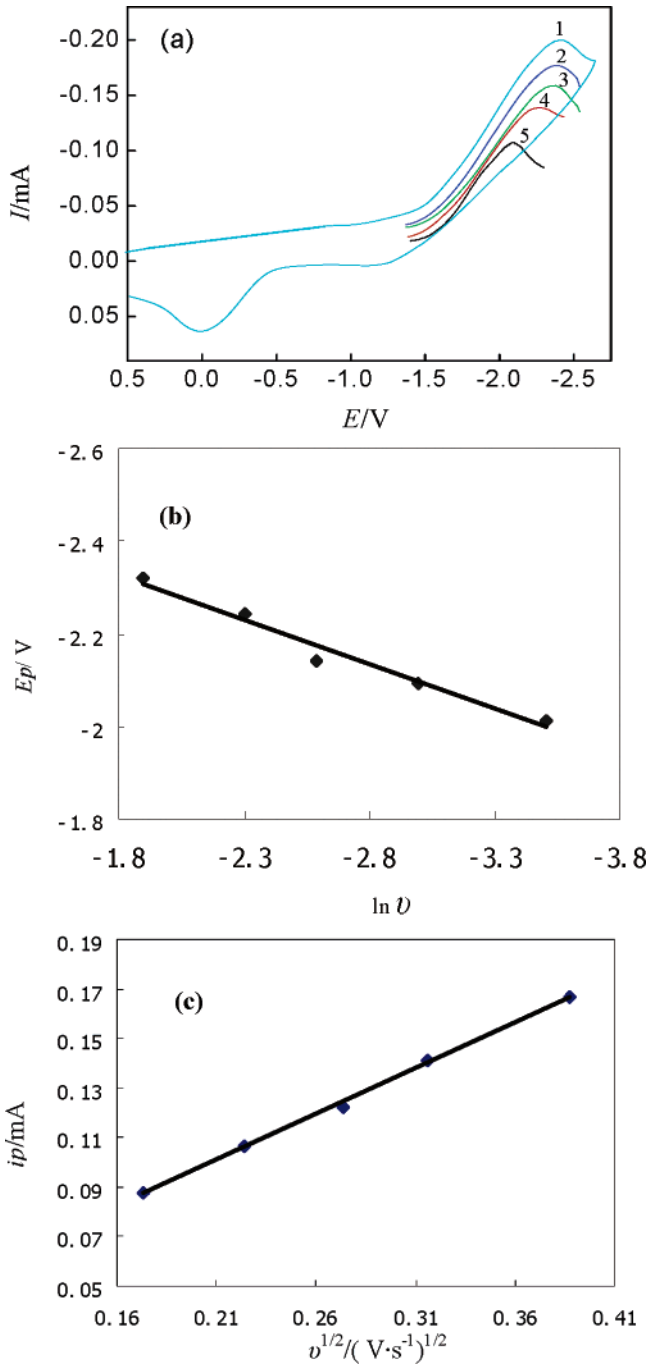

Figure 2. (a) Cyclic voltammograms of Pt electrodes in 0.01 mol/L Ce(CH$_3$SO$_3$)$_3$−3.00 mol/L urea−DMSO (0.08 cm^2) at different sweep rates (T = 298 K, υ/(mV s^{-1}): (1) 200, (2) 150, (3) 100, (4) 50, (5) 30); (b) E_{pc}−ln υ curve; (c) I_p−$\upsilon^{1/2}$curve.

The cyclic voltammograms of Pt electrodes at different sweep rates (υ) in 0.01 mol/L Ce(CH$_3$SO$_3$)$_3$−3.00 mol/L urea−DMSO at 298 K was shown in Figure 2a. There was a cathodic wave appearing in every cyclic voltammogram that corresponded to the reduction of Ce(III), namely, Ce(III) + 3e$^-$ → Ce. The reduction of Ce(III) was irreversible, and a = 0.06 and D = 1.77 × 10^{-10} m^2/s could be obtained according to the data in Figure 2 via a method similar to that above.

Figure 3a shows the cyclic voltammogram of the Cu electrode in the 0.01 mol/L Ce(CH$_3$SO$_3$)$_3$−3.00 mol/L urea−DMSO system at 298 K. One cathodic wave appeared with

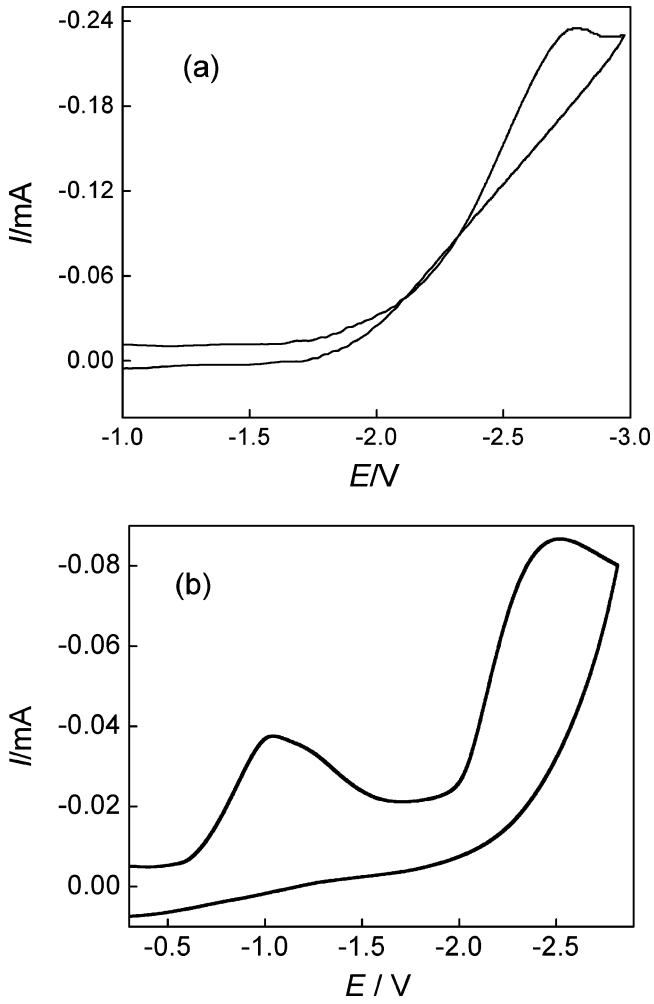

Figure 3. Cyclic voltammograms of Cu electrode in (a) 0.01 mol/L Ce(CH$_3$SO$_3$)$_3$−3.00 mol/L urea−DMSO system and (b) 0.01 mol/L Ce(CH$_3$SO$_3$)$_3$−0.01 mol/L FeCl$_2$−3.00 mol/L urea−DMSO (A = 0.14 cm^2, T = 298 K, υ/(mV s^{-1}) = 50).

a starting potential of −1.85 V, and the peak potential was −2.77 V. It was obvious that the cathodic wave corresponded to the reduction of Ce(III). The cyclic voltammogram of the Cu electrode in the 0.01 mol/L Ce(CH$_3$SO$_3$)$_3$−0.01 mol/L FeCl$_2$−3.00 mol/L urea−DMSO system at 298 K is shown in Figure 3b. There were two cathodic waves appearing in it. The starting potential and peak potential of the first cathodic wave appeared at −0.62 and −1.03 V, respectively. The starting potential and peak potential of the second cathodic wave appeared at −1.94 and −2.50 V, respectively. Comparing with the cyclic voltammogram in Figure 3a, we could easily conclude that the first cathodic wave in Figure 3b corresponded to the electrodeposition of Fe(II) and that the second one corresponded to the electrodeposition of Ce(III). We also could observe that the peak potential of Ce(III) in Figure 3b shifted positively compared with that in Figure 3a. It is obvious that the positive shifting of the peak potential of Ce(III) in Figure 3b was caused by the Fe(II) ions in the urea−DMSO system, which shows that the Fe(II) ions could induce the electrodeposition of Ce(III).

The pure Cu plate with 2.5 cm^2 was chosen as working electrode, and the deposit potential was chosen in the region of −2.00 to −2.80 V. The potentiostatic electrodeposition experiment was carried out in the 0.01 mol/L Ce(CH$_3$SO$_3$)$_3$−

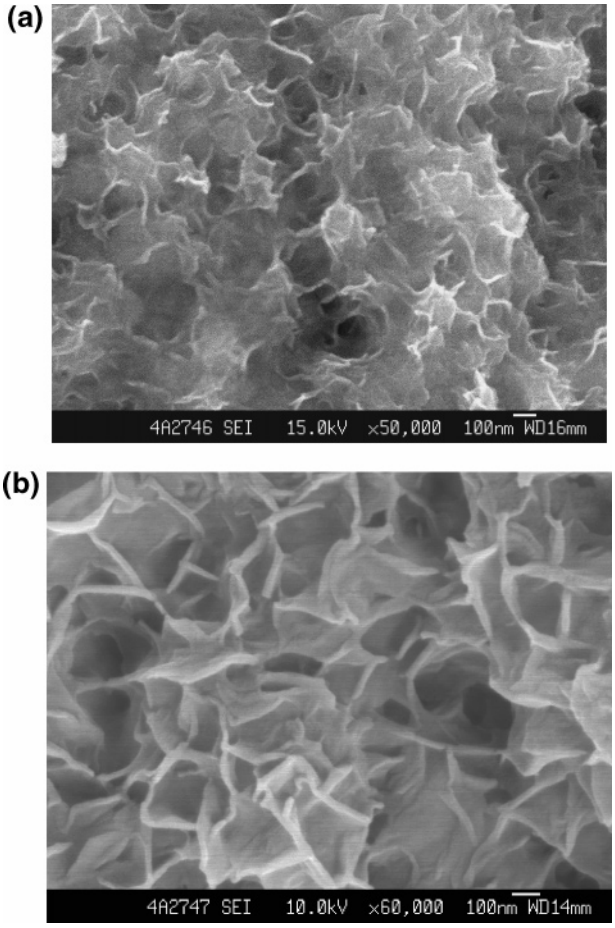

Figure 4. SEM images of the Ce−Fe intermetallic compounds deposited for 30 min in 0.01 mol/L $Ce(CH_3SO_3)_3$−0.01 mol/L $FeCl_2$−3.00 mol/L urea−DMSO system with adding some CH_3COOH that is about 1×10^{-4} mol/L at different deposition potentials. (a) −2.50 V; (b) −2.30 V.

0.01 mol/L $FeCl_2$−3.00 mol/L urea−DMSO system with adding some CH_3COOH that is about 1×10^{-4} mol/L, and the deposition time is 30 min. Images a and b of Figure 4 show the typical SEM images of Ce−Fe intermetallic compounds with foam structures deposited at −2.50 and −2.30 V, respectively. It can be seen that the surfaces are composed of numerous nanosized pores that lead to high superficial volume and low density. The sizes of the pores in images a and b of Figure 4 are about 150−300 and 100−200 nm, respectively. The thicknesses of the walls in images a and b of Figure 4 are about 10 and 15 nm, respectively. Interestingly, we found that the deposit shown in Figure 4b had more pores than that shown in Figure 4a. Moreover, it was also found that the wall structure, i.e., morphology of the branches, of the deposit shown in Figure 4b was better than that shown in Figure 4a. The above results suggest that increasing deposition potential simply reduces the electrodeposition rate, which has a very favorable effect on the pore number and wall structure of the foam. The XRD diffraction peaks of the deposition film were observed within the range scanning of $2\theta = 20-80^{o}$. No diffraction peaks were found in the XRD pattern besides the peaks of the copper substrate, as shown in Figure 5, which suggested that the film was amorphous.

The formed structures can be explained by the hydrogen bubbles functioning as a dynamic template during metal

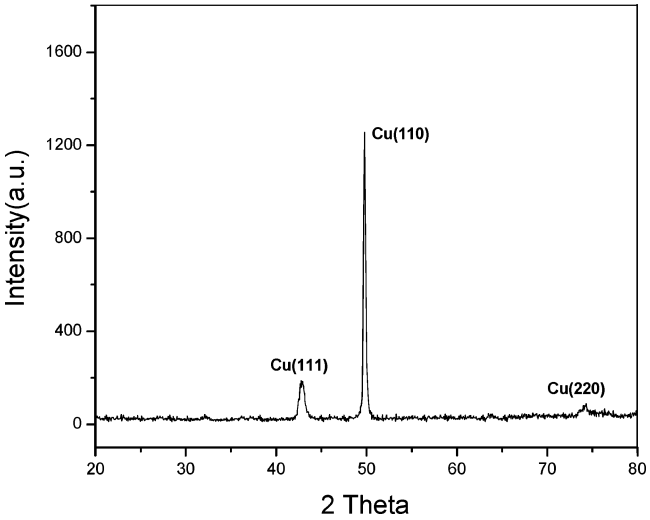

Figure 5. XRD patterns of the prepared Ce−Fe intermetallic compounds with foam structures.

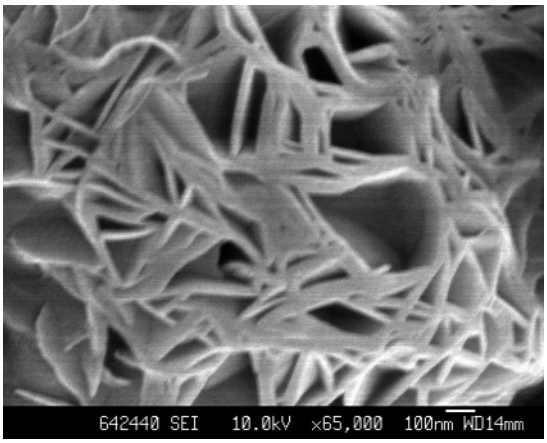

Figure 6. SEM images of the Ce−Fe intermetallic compounds deposited for 30 min in 0.05 mol/L $Ce(CH_3SO_3)_3$−0.01 mol/L $FeCl_2$−3.00 mol/L urea−DMSO system with adding 2×10^{-4} mol/L CH_3COOH at −2.30 V.

deposition. Because the electrodeposition potential is very negative (at −2.00 to −2.80 V), a large number of hydrogen bubbles created on the copper substrate move toward the electrolyte/air interface during the electrodeposition process when CH_3COOH is added into the deposition solution. Therefore, the metal growth toward the gas bubble is prohibited simply because there are no metal ions available there, which lead to the deposition happening only between gas bubbles. In the end, the porous structures will be formed with increasing electrodeposition time. To increase the number of the pores, there are two methods that can be utilized. The foam structure is caused by the competitive reaction of the electrodeposition and hydrogen evolution. This implies that either increasing the H_2 evolution rate (by increasing the concentration of hydrogen ions) or reducing the electrodeposition rate (by reducing the concentration of the salts) may be an effective approach to increasing the number of the pores. Figure 6 shows the foam structures deposited in the 0.05 mol/L $Ce(CH_3SO_3)_3$−0.01 mol/L $FeCl_2$−3.00 mol/L urea−DMSO system with 2×10^{-4} mol/L CH_3COOH at a deposition potential of −2.30 V. The wall thicknesses of the pores obviously increase with increasing concentration of $Ce(CH_3SO_3)_3$ in deposition

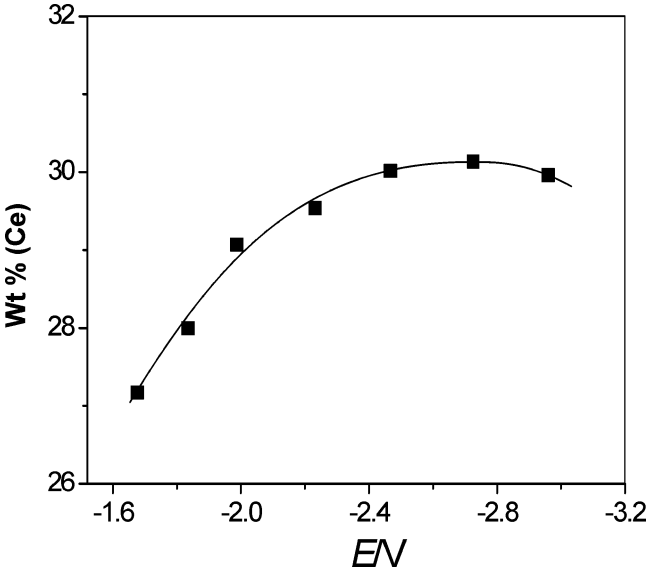

Figure 7. Effect of deposition potentials on the Ce contents in Ce−Fe thin films.

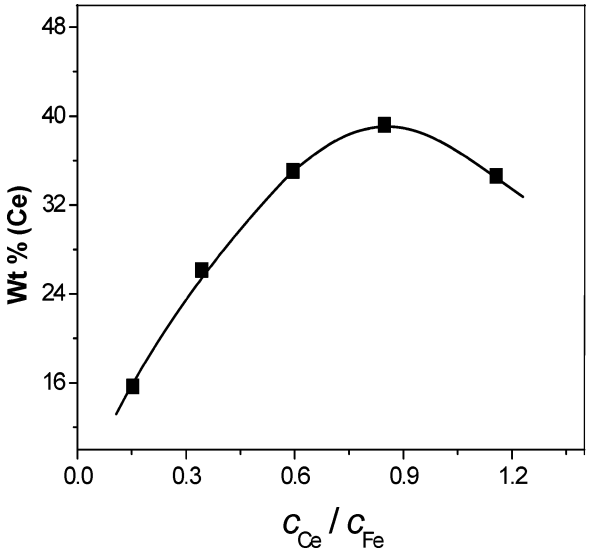

Figure 8. Effect of the ratio of Ce(III) and Fe(II) on the Ce contents in Ce−Fe thin films.

solution compared to that in Figure 4b; the density of pores also increases with the concentration of CH_3COOH.

The compositions of deposits were analyzed by the means of EDS and the results are shown in Figure 7. The data in Figure 7 suggests that the contents of Ce in Ce−Fe intermetallic compounds increased at first and then decreased when the electrodeposition potential shifted negatively. The reason can be explained as following. With the potentials of electrodeposition shifted negatively, the rates of electrodeposition of Ce^{3+} increased, and the concentration polarizations also increased. However, when the potential of electrodeposition was negative to −2.70 V, it would lead to the rate of electrodeposition being badly influenced by the concentration polarization. This causes the rate of electrodeposition of Ce^{3+} to decrease and thus results in the content of Ce in Ce−Fe intermetallic compounds decreasing. The effect of Fe^{2+} concentration in the solution on the Ce content of the deposit was also studied. It is obvious that the lower Fe^{2+} concentration in the solution, the higher the Ce content in the deposit will be obtained. However, the system will become rather unstable when the Fe^{2+} concentration in the solution is very low, greatly reducing the rate of co-deposition of Fe^{2+} and Ce^{3+}. So, the Fe^{2+} concentration in the solution should be maintained in the suitable range 0.01−0.2 mol/L for getting preferable Ce−Fe intermetallic compounds. The effect of the ratios of the concentrations of Ce^{3+} to Fe^{2+} in the deposition solution on Ce content in the deposit was also studied, and the result is shown in Figure 8. The content of Ce almost reached the maximum when $c_{Ce}/c_{Fe} = 4$ in the solution. The reason may be that the reduction potential of Ce^{3+} becomes positive with increasing the concentration of Ce^{3+} when it is in the relatively low concentration range. This causes the content of Ce in the film to increase. However, when the concentration of Ce^{3+} is further increased, it changes the ratio of the concentrations of Ce^{3+} to Fe^{2+} in the deposition solution, and the relative concentration of Fe^{2+} is decreased. The reduction potential of Ce^{3+} becomes more positive with increasing Ce^{3+} concentration, which is favorable to increasing the content of Ce in the deposits; however, the induced effect of Fe^{2+} for the electrochemical reduction of Ce^{3+} is decreased relative to the decrease in concentration of Fe^{2+} in deposition solution. Therefore, this will cause the content of Ce in the deposits to reach the maximum and then to decrease with increasing Ce^{3+} concentration.

4. Conclusions

The electrode processes of Fe(II) and Ce(III) reducing on Pt electrodes were irreversible steps. Experimental results showed that Fe(II) in 3.00 mol/L urea−DMSO could induce the electrodeposition of Ce(III). The high surface area of Ce−Fe intermetallic compounds with porous nanostructures could be prepared by potentiostatic electrodeposition with deposition potentials of −2.00 to −2.80 V. The concentrations of the salts and hydrogen ions have much effect on the pore number and wall structure of the foam. Increasing the H_2 evolution rate by increasing the concentration of hydrogen ions or reducing the electrodeposition rate by reducing the concentration of the salts was an effective approach to increasing the number of the pores. The deposits have more surface pores and better wall structures with increasing deposition potentials. The content of Ce in Ce−Fe intermetallic compounds increased at first and then decreased when the deposition potential shifted negatively. The electrodeposited Ce−Fe intermetallic compounds were amorphous, as proved by X-ray diffraction analysis.

Acknowledgment. This work was supported by the Natural Science Foundations of China (Grants 20603048 and 20573136), the Natural Science Foundations of Guangdong Province (Grants 06300070, 06023099, and 04205405), and the Foundations of Potentially Important Natural Science Research and Young Teacher Starting Up Research of Sun Yat-Sen University.

Note Added after ASAP Publication. There was missing data in Figure 1 in the version published ASAP April 4, 2007; the corrected version was published ASAP April 6, 2007.

CM062206Q